Annealing-Induced Chemical Interaction at the Ag/In$_2$O$_3$:H Interface as Revealed by In Situ Photoelectron Spectroscopy

Ting Xiao, Darja Erfurt, Roberto Félix, Xiaxia Liao, Johannes Frisch, Daniel Abou-Ras, Katherine A. Mazzio, Regan G. Wilks, Rutger Schlatmann, and Marcus Bär*

Hydrogen-doped In$_2$O$_3$ (In$_2$O$_3$:H) is highly conductive while maintaining extraordinary transparency, thus making it a very attractive material for applications in optoelectronic devices such as (multijunction) solar cells or light-emitting devices. However, the corresponding metal/In$_2$O$_3$:H contacts may exhibit undesirably high resistances, significantly deteriorating device performance. To gain insight into the underlying efficiency-limiting mechanism, hard X-ray photoelectron spectroscopy is employed to in-situ monitor annealing-induced changes in the chemical structure of the Ag/In$_2$O$_3$:H interface system that is further complemented by ex-situ electron microscopy analyses and contact resistance measurements. The observed evolution of the Ag- and In-related photoelectron line intensities can be explained by significant intermixing across the Ag/In$_2$O$_3$:H interface. The corresponding lineshape broadening of the Ag 3d spectra is attributed to the formation of Ag$_2$O and AgO, which becomes significant at temperatures above approximately 160 °C. However, after annealing to 300 °C, instead of the formation of an insulating AgO$_x$ interfacial layer, it is found i) In to be rather homogeneously distributed in the complete Ag/In$_2$O$_3$:H stack, ii) Ag diffusing into the In$_2$O$_3$:H, and iii) an improvement of the contact resistance rather than its often-reported deterioration.

1. Introduction

Hydrogen-doped In$_2$O$_3$ (In$_2$O$_3$:H) is a very promising candidate for transparent conductive oxides (TCOs) as used in, for example, optoelectronic devices, due to a relatively high electron mobility of >130 cm^2 V^{-1} s^{-1}[1] and a suitable carrier density in the 10^{20} cm^{-3} range. It has been successfully implemented in optoelectronic devices, such as (multijunction) solar cells or light-emitting devices, as transparent contact. Together with the employed metal electrodes, it is supposed to provide an Ohmic contact ideally resulting in (almost) lossless current transport. However, a high contact resistance is observed for the Ag/In$_2$O$_3$:H layer stack after performing a post-annealing treatment (usually at around 200 °C required to cure the screen-printed silver paste generally used to form the front grid of respective solar cells).[2] The metal/In$_2$O$_3$:H interface

T. Xiao, R. Félix, X. Liao, J. Frisch, R. G. Wilks, M. Bär
Department of Interface Design
Helmholtz-Zentrum Berlin für Materialien und Energie GmbH (HZB)
Albert-Einstein-Str. 15, 12489 Berlin, Germany
E-mail: marcus.baer@helmholtz-berlin.de

D. Erfurt, R. Schlatmann
PVcomB
Helmholtz-Zentrum Berlin für Materialien und Energie GmbH (HZB)
Schwarzschildstraße 3, 12489 Berlin, Germany

X. Liao
School of Physics and Materials Science
Nanchang University
Nanchang 330031, P. R. China

D. Abou-Ras
Department of Structure and Dynamics of Energy Materials
Helmholtz-Zentrum Berlin für Materialien und Energie GmbH (HZB)
Hahn-Meitner-Platz 1, 14109 Berlin, Germany

K. A. Mazzio
Department of Chemistry
Humboldt University of Berlin
Brook-Taylor-Str. 2, 12489 Berlin, Germany

K. A. Mazzio
Joint Research Group Operando Battery Analysis
Helmholtz-Zentrum Berlin für Materialien und Energie GmbH
Hahn-Meitner-Platz 1, 14109 Berlin, Germany

R. G. Wilks, M. Bär
Energy Materials In-situ Laboratory Berlin (EMIL)
Helmholtz-Zentrum Berlin für Materialien und Energie GmbH
Albert-Einstein-Str. 15, 12489 Berlin, Germany

R. Schlatmann
Hochschule für Technik und Wirtschaft Berlin
Treskowallee 8, 10318 Berlin, Germany

M. Bär
Department of X-ray Spectroscopy at Interfaces of Thin Films,
Helmholtz-Institute Erlangen-Nürnberg for Renewable Energy (HI ERN)
Albert-Einstein-Str. 15, 12489 Berlin, Germany

M. Bär
Department of Chemistry and Pharmacy
Friedrich-Alexander-Universität Erlangen-Nürnberg
Egerlandstr. 3, 91058 Erlangen, Germany

(e.g., Ag,[3] Pt,[4] and Pb[4]/In$_2$O$_3$) can behave as a Schottky contact if not designed carefully, which may have a considerable impact on the macroscopic behavior of the final device. For In$_2$O$_3$, it is generally assumed that the electron accumulation layer that is formed at the surface prevents the formation of rectifying Schottky contacts.[4a] However, high resistivity Schottky-type metal/In$_2$O$_3$ contacts have been reported. In addition, for the Ag/In$_2$O$_3$:H layer stack, Barraud et al.[2] suggest that the high contact resistance may be related to the formation of an insulating interfacial layer (i.e., Ag$_2$O) rather than the formation of a Schottky-type contact. Whereas, Xu et al.[5] report an improved contact resistance at the indium-zinc-oxide (IZO) homojunction interface by introducing Ag nanoparticles. At this point, a better understanding of how the Ag/In$_2$O$_3$:H interface forms and what role the potential post-annealing induced (out)diffusion of hydrogen from the In$_2$O$_3$:H plays[6] is crucial for the In$_2$O$_3$:H material system to mature as a credible TCO alternative. In this work, we study the Ag/In$_2$O$_3$:H interface formation and how it is impacted by post-annealing. Hard X-ray photoelectron spectroscopy (HAXPES) was employed to investigate the chemical structure of the (deeply buried) Ag/In$_2$O$_3$:H interface and—to mimic the heat input during subsequent process steps in device preparation—how it changes upon in-situ annealing from room temperature to 300 °C. These measurements were complemented by scanning (SEM) and transmission electron microscopy (TEM) measurements of the annealed Ag/In$_2$O$_3$:H sample. Furthermore—to directly be able to relate the findings to the electrical properties—the contact resistance of an Ag/In$_2$O$_3$:H stack was determined.

We find a distinct impact of the post-annealing temperature on the structure of the Ag/In$_2$O$_3$:H interface. While changes in sample topography seem to prevail at low post-annealing temperatures <160 °C, the formation of Ag—O bonds is the main effect in the intermediate temperature regime between 160 and 215 °C, and In diffusion becomes dominant in the high-temperature regime >215 °C. Notably, high-temperature post-annealing treatments at 300 °C lead to a significantly improved contact resistance, contrary to the reported effects when using lower-temperature post-annealing.[2,4]

2. Results and Discussion

The HAXPES survey spectrum of the as-deposited thin Ag/In$_2$O$_3$:H sample (see Figure S4, Supporting Information) indicates that Ag-related photoelectron and Auger lines dominate the spectrum, as well as In and O-related signals are significantly attenuated (as expected). In addition, a C 1s signal can be observed, which is attributed to carbon present in a surface contamination layer and/or incorporated into the metal film. In addition, we find the presence of aluminum (Al 1s), which we ascribe to contamination from the Al$_2$O$_3$ crucible used in the electron beam evaporator (see discussion in conjunction with Figure S4, Supporting Information, for more details).

Figure 1 shows the Ag 3d spectra of an Ag/In$_2$O$_3$:H sample in-situ monitored during annealing from room temperature to 300 °C in ultra-high vacuum (UHV) conditions. In the main panel (Figure 1b), the temperature evolution of the Ag 3d$_{3/2}$ and Ag 3d$_{5/2}$ spin-orbit doublet can be clearly observed. While
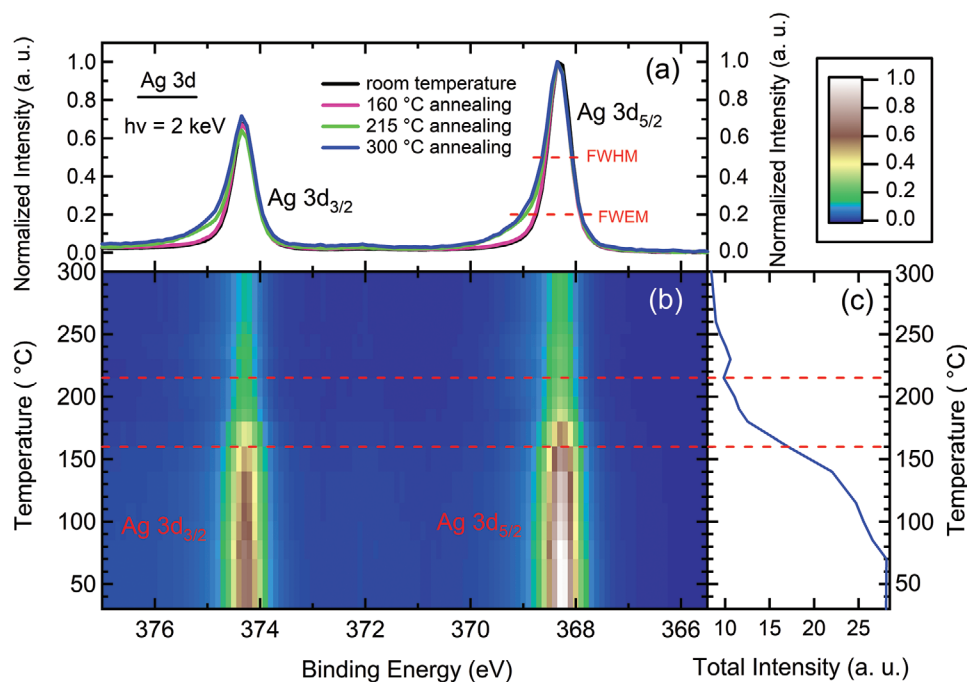

Figure 1. a) Hard X-ray photoelectron spectra of the Ag 3d region of the Ag/In$_2$O$_3$:H sample at different annealing temperatures recorded in-situ with an excitation energy of 2 keV. b) Corresponding color-coded intensity map of Ag 3d spectra as a function of post-annealing temperature. c) Evolution of the Ag 3d line intensity in the shown range during in-situ annealing. The spectra in panel (a) are normalized to uniform peak and background heights, and the data in panel (b) are normalized to the background at 366.5 eV. The total intensity depicted in panel (c) is derived from the normalized data shown in panel (b). The horizontal dashed red lines in panels (b) and (c) are guides to the eye and indicate temperatures of 160 and 215 °C.
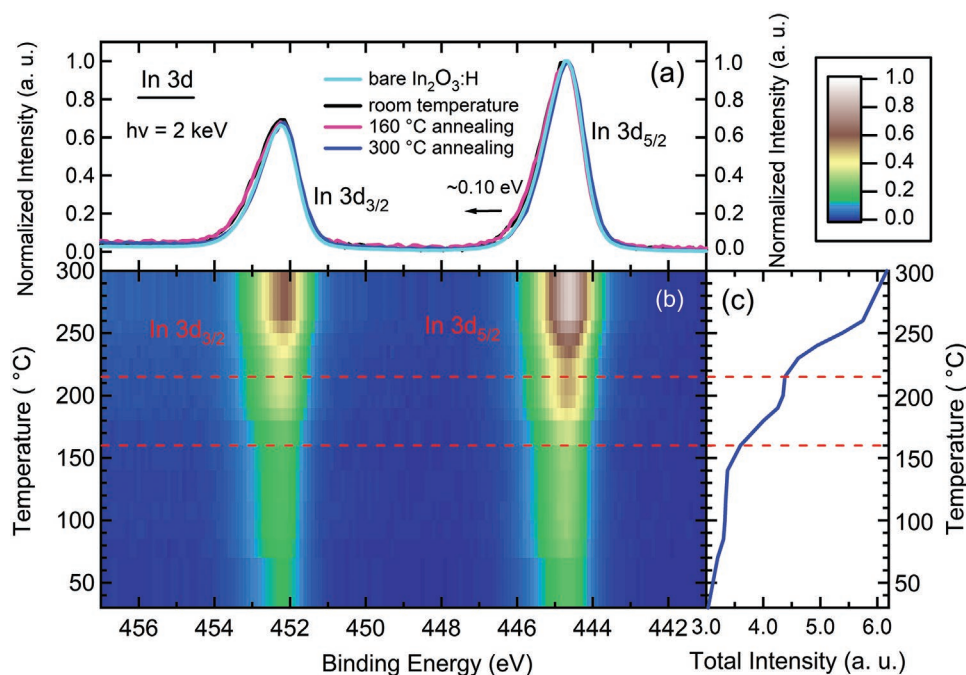
2202347 (2 of 8)

**ADVANCED
SCIENCE NEWS**

www.advancedsciencenews.com

**ADVANCED
MATERIALS
INTERFACES**

Open Access

www.advmatinterfaces.de

Figure 2. a) Hard X-ray photoelectron spectra of the In 3d region of room temperature bare In_2O_3:H and of Ag/In_2O_3:H at different annealing temperatures measured with an excitation energy of 2 keV. b) Corresponding color-coded intensity map of In 3d spectra as a function of temperature. c) Evolution of the In 3d line intensity in the shown range during annealing. The spectra in panel (a) are normalized to uniform peak and background heights, and the data in panel (b) are normalized to the background at 442.5 eV. The total intensity depicted in panel (c) is derived from the normalized data shown in panel (b). The horizontal dashed red lines in panels (b) and (c) are guides to the eye and indicate temperatures of 160 and 215 °C.

Figure 1c shows that a decrease in Ag signal already starts at an annealing temperature of ≈75 °C, a sharp drop in intensity occurs between 160 and 215 °C. To better illustrate the spectral lineshape changes, exemplarily Ag 3d spectra of the Ag/In_2O_3:H sample at room temperature, 160, 215, and 300 °C are plotted normalized to uniform peak and background heights in Figure 1a. This allows to clearly observe the asymmetric broadening toward higher binding energies (up to around 369 eV for the $3d_{5/2}$ line, see Figure 1a) that manifests in an increase of the full width at half maximum (FWHM) (more obvious for the full width at one-eighth maximum [FWEM], see also Figure 3a) of the Ag 3d line upon annealing. The position and spectral shape of the Ag 3d line at room temperature and 160 °C are consistent with metallic Ag,[7] indicating that Ag is mainly present in a metallic state at the start of the annealing experiment. Above 160 °C, and concurrent with the overall decrease in Ag 3d peak intensity (see Figure 1c), the noticeable asymmetric peak broadening indicates a change in the chemical environment of Ag, for example, the formation of new species, interdiffusion, or changing surface-to-volume ratios (as further discussed below). Note that the peak position of the intensity maximum shows no appreciable systematic change upon temperature increase.

The evolution of the In 3d spectra during the in-situ annealing experiment is present in **Figure 2**. The general trend of the increasing In 3d intensity with rising temperature (Figure 2b,c) is mainly in agreement with the decreasing Ag 3d signal (see Figure 1b,c), at least until 215 °C. The Ag 3d line intensity drops significantly between 160 and 215 °C, which relates to the strong In 3d line intensity increase in the same temperature regime. However, for temperatures >215 °C, an

even steeper In 3d line intensity increase is observed, while the (already reduced) Ag 3d intensity does not change significantly (see Figure 1c). The direct comparison of the In 3d spectra of the bare In_2O_3:H with the Ag/In_2O_3:H sample at room temperature (Figure 2a) reveals a small shift (≈0.10 eV) toward higher binding energies; upon sample annealing, the In 3d binding energy shifts back toward that of the In 3d position of the bare In_2O_3:H sample. Furthermore, all of the In 3d core-level peaks display a strong asymmetry (Figure 2a), as has been previously reported in the spectra of other post-transition metal oxides[8] and often attributed to final-state effects during the photoelectron process.[9] While with Ag deposition, a small broadening in the spectral shape of the In 3d line is observed for Ag/In_2O_3:H compared to that of the bare In_2O_3:H, some continuous narrowing of the In 3d core level line occurs upon annealing (see also **Figure 3**a).

The SEM image of the Ag/In_2O_3:H sample after in-situ annealing to 300 °C in Figure S5, Supporting Information, shows that the Ag has formed particles on the surface in agreement with the observations on IZO by Xu et al.[5] Particle formation is unsurprising also in this studied case considering the related surface and interface energies that govern the layer topography: Based on literature data of In_2O_3 (for details see Section S4, Supporting Information), we expect the surface energy of In_2O_3:H[10] to be significantly smaller than the average surface energy of Ag[11] and thus an island-type (Vollmer–Weber) growth is expected. Hence, for all samples including the as-deposited Ag/In_2O_3:H, the topography might be best described by small Ag islands instead of by a closed Ag film covering the In_2O_3:H. This model agrees well with the
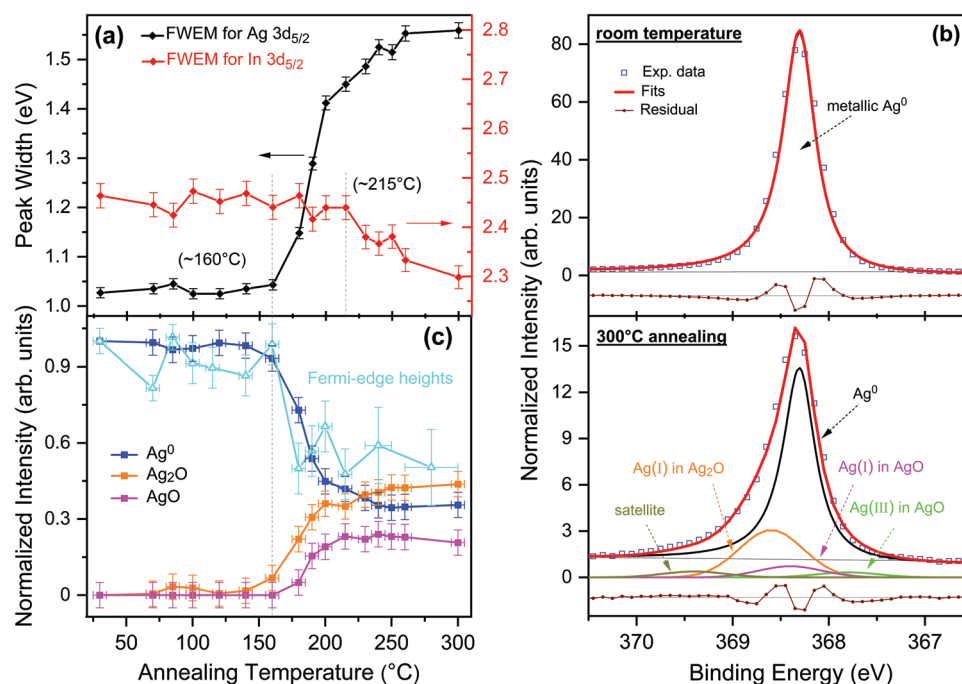
Figure 3. a) Full width at one-eighth maximum (FWEM) of Ag $3d_{5/2}$ and In $3d_{5/2}$ spectra as a function of annealing temperature. b) Example fits of the Ag $3d_{5/2}$ spectra of the room temperature and 300 °C Ag/In$_2$O$_3$:H sample following the approach suggested in ref. [12]. c) Evolution of the relative contributions of metallic Ag (Ag^0) (blue line), Ag$_2$O (orange line), and AgO (magenta line) to the Ag $3d_{5/2}$ line with annealing temperature in comparison to the relative height of the Fermi-edge (cyan line) as derived from the in situ HAXPES measurements ($h\nu$ = 2 keV, see Figure S9, Supporting Information). The HAXPES-derived Fermi-edge heights are shown as a function of the mean annealing temperature with the respective x-axis error bars indicating the temperature ranges in which respective spectra have been added up to improve statistics (see Supporting Information for more details).

HAXPES data (see discussion in conjunction with Figure S4, Supporting Information). Note that while island formation seems to be problematic for providing good electrical contact, Xu et al.[5] have found an improved contact resistance at the IZO homojunction interface by introducing Ag nanoparticles. Moreover, in some applications, the formation of point contacts of Ag islands might be of advantage/desired (e.g., to additionally improve the transparency of the contact and/or reduce interface recombination). Also note that in "real-world" applications (as in the case of using screen-printed contacts), significantly thicker Ag layers are deployed, and it can be expected that the initially formed islands coalesce into a closed layer in these cases, consistent with the good conductivity measured for corresponding as-deposited samples (see Figures S2 and S3 and Table S2, Supporting Information).

The island-type topography could to some extent explain the observed increase of the In 3d (see Figure 2) and decrease of the Ag 3d (see Figure 1) line upon annealing, assuming that the Ag islands formation is induced/enhanced or there is an increased agglomeration of the Ag islands upon heat treatment. Especially in the low-temperature regime below 160 °C where they are strongly correlated (although slight relative to the changes at a higher temperature) with increases of the In 3d and decreases of the Ag 3d line intensities, this scenario appears to be most likely. However, based on a detailed (semi-quantified) consideration of the identified layer topography (see discussion in conjunction with Figure S5, Supporting Information, for details) also annealing-induced interdiffusion processes have to be considered, in particular at higher post-

annealing temperatures. This is corroborated by TEM analysis of the cross-section of the Ag/In$_2$O$_3$:H sample that had been in-situ annealed to 300 °C (see Figure S6, Supporting Information), showing that basically In and Ag are homogeneously distributed across the complete Ag/In$_2$O$_3$:H layer stack cross-section (i.e., In is present in the particles initially ascribed to Ag and Ag is present across the In$_2$O$_3$:H layer).

The proposed interdiffusion processes can be better understood by more closely analyzing the spectral shape changes of the Ag 3d and In 3d lines observed in Figures 1 and 2. The Ag 3d line changes with annealing temperature, becoming broader at high temperatures, and the changes are visualized in Figure 3a, where the Ag $3d_{5/2}$ FWEM values of the spectra from Figure 1 are shown as a function of annealing temperature (FWEM is chosen to accentuate the emergence of the higher binding energy shoulder, which has a negligible effect on the more standard FWHM). The broadening in the Ag $3d_{5/2}$ spectra begins at around 160 °C and continues up to a temperature of 215 °C—the same temperature regime in which the Ag 3d intensity drops significantly (see Figure 1). This indicates the formation of additional Ag species during annealing and presumed diffusion into the In$_2$O$_3$:H, as evidenced by the TEM analysis (see Figure S6, Supporting Information) discussed above.

Figure 3b shows the curve fit results of the Ag $3d_{5/2}$ spectra for the room temperature and the 300 °C Ag/In$_2$O$_3$:H sample, in agreement with (exclusively) metallic Ag being present in the sample before annealing and a significant Ag oxidation taking place upon post-annealing to 300 °C. The complex lineshape of

the Ag 3d spectra of Ag oxide contributions requires that multiple peaks be used to represent the spectrum of AgO. The fit procedure was derived in accordance with ref. [12], a detailed description of the procedure is provided in Supporting Information and Figures S7 and S8, Supporting Information. An asymmetric Doniach–Sunjic profile[13] is used for fitting the metallic Ag (Ag^0) contribution, and symmetric Voigt profiles are employed to represent the Ag oxides (Ag_2O and AgO). The spectrum of the room temperature Ag/In_2O_3:H sample shows a single peak attributed to Ag^0, while the 300 °C-annealed Ag/In_2O_3:H spectrum is composed of a mixture of Ag^0 and ($Ag_2O + AgO$). Because of the change in the overall amount of Ag, it is important to closely examine the applied fit model and spectra to determine whether the absolute quantity of oxidized Ag truly increases with temperature, or if the clear relative increase in oxide concentration is due only to a disappearance of the metallic Ag. Several fit models are described and present in Figures S7 and S8, Supporting Information, and they strongly indicate that the quantity of oxidized Ag does in fact increase upon annealing in absolute terms.

Figure 3c shows the fit-derived intensities (for details see Figure S8, Supporting Information) of the Ag^0, Ag_2O, and AgO contributions to the Ag 3d line for the Ag/In_2O_3:H sample as a function of annealing temperature. The drop in overall intensity around 160 °C, described above, is mainly caused by the reduced intensity of the Ag^0 signal. This is in agreement—within the experimental uncertainty—with the evolution of the Fermi-edge (E_F) height used as a fit-model-independent approach to quantify the fraction of Ag which remains in a metallic state (see Figure S9, Supporting Information, for details) and thus confirms the validity of the employed fit model discussed above and in Supporting Information (see Figures S7 and S8, Supporting Information). While the addition of a small Ag_2O component is required to obtain reasonable fits in some spectra measured at temperatures below 100 °C, significant contributions of Ag_2O and AgO appear in the spectra measured at temperatures above 160 °C. Both oxide contributions increase up to an annealing temperature of around 215 °C and level off at higher temperatures. This is consistent with the lineshape broadening in the Ag 3d spectra occurring at the same temperature (≈160 °C) and leveling off at ≈215 °C.

Koida et al.[6] report on thermal desorption spectroscopy (TDS) measurements of different In_2O_3:H samples that had been solid-phase crystallized at different temperatures, and their findings provide some necessary context for the above observations. For In_2O_3:H that had undergone crystallization treatment at temperatures ≤160 °C, significant amounts of physisorbed and hydrogen-bonded water desorb at 70 and 135 °C, respectively (note that H_2O is used in the deposition process to provide the hydrogen doping of the In_2O_3, see Experimental Section below). If In_2O_3:H is crystallized at temperatures above 160 °C, most of the water desorbs above 170 °C as it must first "prediffuse" to the surface.[6] Prior to Ag deposition, the In_2O_3:H in the current experiment had been annealed at 200 °C as part of the solid-phase crystallization process, hence the chemical changes at lower temperatures are limited to the modification of topography (i.e., agglomeration of Ag). In Figure 3c, we see a small increase in Ag oxide concentration at lower temperatures (<100 °C); the larger, steeper increase in Ag

oxide contribution occurs at the higher temperature threshold (160 °C). This oxidation might be related to further water desorption (and thus is in agreement with the TDS measurements) considering that oxidation of Ag can occur according to $2Ag + 2H_2O \rightarrow 2AgOH + H_2$ and a) $2AgOH \rightarrow Ag_2O + H_2O$ and/or b) $2AgOH \rightarrow 2AgO + H_2$. Based on the enthalpies of formation, both reactions are predicted to be thermodynamically favorable, with Ag_2O ($\Delta Hf\_Ag_2O = -31.1$ kJ mol^{-1})[14] being slightly more favorable to form than AgO ($\Delta Hf\_AgO = -24.3$ kJ mol^{-1}),[14] in agreement with the derived Ag_2O and AgO contributions to the Ag $3d_{5/2}$ line in Figure 3c.

The FWEM of the In $3d_{5/2}$ spectra from Figure 2 is shown as a function of annealing temperature in Figure 3a. The change is significantly less pronounced than the corresponding change in Ag $3d_{5/2}$; nevertheless, a gradual decrease occurs above 215 °C, that is, the temperature for which a steep In 3d intensity increase is observed (see Figure 2). The change is likely due either to further dehydration of (potentially still present) indium hydroxide occurring upon vacuum annealing[6] or to In-related diffusion processes (as evidenced by the TEM images in Figure S6, Supporting Information) taking place in the high post-annealing temperature regime. In that context, it should be considered that asymmetric lineshapes may not necessarily indicate chemical shifts due to the presence of multiple species (as in the case of the Ag 3d line). Final-state screening effects, for example, have been proposed as the cause of asymmetric lineshapes observed in XPS core-level data of highly conductive metal oxides, such as Sn-doped In_2O_3,[8f] Sb-doped SnO_2,[8a,b] and Na_xWO_3,[8e] and so it is possible that the asymmetric peak shape of the In 3d line (and its annealing-induced change) could also be interpreted in this framework. This final-state screening model would then suggest that the decreasing In 3d FWEM for annealing temperatures >215 °C indicates a decreasing electron density (see discussion in conjunction with Figure S10, Supporting Information, for more details), which may be accounted for by the formation of In vacancies in the In_2O_3:H layer due to the (out)diffusion of In into Ag. In vacancies can act as compensation centers in In_2O_3, leading to n-type carrier (i.e., electron) reduction.[15] In this temperature regime, a certain amount of Ag may also diffuse into the In_2O_3:H layer (as corroborated by the TEM images in Supporting Information and the continued slight decrease of the Ag 3d line in this temperature regime—see Figure 1). Once Ag atoms are incorporated into the In_2O_3:H layer, they can be stabilized in an interstitial site (more favorable) or a position substitutional to In. In both cases, the Ag impurities mainly adopt a +1 oxidation state and the lineshape of the corresponding Ag 3d spectrum would be expected to be similar to that of Ag_2O (i.e., a single symmetric peak rather than the asymmetric peak of Ag^0 or the complex structure of AgO). The resulting acceptor-like Ag^+ derived states in In_2O_3:H would, similar to the In vacancies, also lead to a reduction of the net concentration of n-type charge carriers, which, according to the screening model, would also contribute to the narrowing of the In 3d line. Both the formation of In vacancies and the presence of Ag^+ states (induced by high temperature-promoted diffusion processes) then also explain the shift of the In 3d line to lower binding energies upon annealing in this post-annealing temperature regime (see Figure 2a).

2202347 (5 of 8)

ADVANCED
SCIENCE NEWS
www.advancedsciencenews.com

ADVANCED
MATERIALS
INTERFACES
Open Access
www.advmatinterfaces.de

It has been speculated that the high contact resistance observed for the Ag/In$_2$O$_3$:H interface after performing a post-annealing treatment may be related to the formation of an insulating interfacial layer (i.e., Ag$_2$O).[2] We do find evidence for the formation of silver oxide(s) in the Ag 3d spectra; however, TEM analysis (see Figure S6, Supporting Information) does not indicate the formation of an interfacial AgO$_x$ layer for the Ag/In$_2$O$_3$:H sample annealed to 300 °C. We find a rather homogeneous distribution of In throughout the complete Ag/In$_2$O$_3$:H layer stack and consequently also Ag diffusion into the In$_2$O$_3$:H after annealing. The comparison to the previous findings is not exact; the discrepancy may be due to the higher annealing temperature (300 °C) and longer annealing times (rather hours than minutes) we used for our study. Usually, the post-annealing treatment to cure the screen-printed Ag paste (which also typically includes a suspension matrix/solvent that could provide an additional oxygen source under annealing, depending on its composition) is performed for a few minutes at 200 °C, a temperature we find to be in the "critical" temperature regime between 160 and 215 °C, where we find the biggest change with respect to intensity and width of the Ag 3d line (see Figure 1). Thus, already small temperature fluctuations will have a significant impact on the chemical interface structure. Furthermore, if the related processes of Ag diffusion and AgO$_x$ formation are in any way kinetically limited, the duration of the post-annealing treatment could also be critically decisive for the resulting interface structure. Also, the steepest intensity change of the In 3d line is observed for temperatures >215 °C (see Figure 2). Hence, one might speculate that at this temperature, the unfavorable scenario of having an insulating AgO$_x$ (or In$_2$O$_3$ heavily compensated by diffused Ag) interface layer resulting in a deterioration of the contact resistance is converted into the beneficial scenario of having a homogeneous In distribution in the whole Ag/In$_2$O$_3$:H stack and Ag diffusion into the In$_2$O$_3$:H, resulting in improved contact resistance (as depicted in **Figure 4**). As a matter of fact, if a post-annealing temperature of 300 °C is used, we find an improved contact resistance: 3–6 × 10^{-5} Ω cm^2 (compared to 1–1.5 × 10^{-3} Ω cm^2 for the as-deposited Ag/In$_2$O$_3$:H contact, see Figures S2 and S3 and Table S2, Supporting Information, for details). However, further dedicated studies are required to confirm this hypothesis.
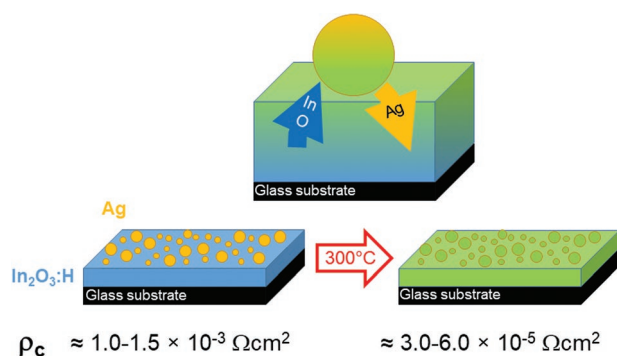

Figure 4. Artist view of the observed annealing-induced changes of the chemical structure of the Ag/In$_2$O$_3$:H stack and the underlying diffusion processes suggested by the present data. The impact on the contact resistance (ρ_c) is also depicted.

3. Conclusion

The chemical structure of the Ag/In$_2$O$_3$:H and how it changes upon annealing to 300 °C has been in-situ monitored by HAXPES in combination with ex-situ electron microscopy analyses. Upon annealing, the Ag 3d line intensity significantly decreases in intensity and broadens while the In 3d line intensity increases and narrows. SEM images reveal the formation of an island-type (Vollmer–Weber) Ag topography on the In$_2$O$_3$:H after post-annealing to 300 °C. In conjunction with the temperature-dependent variation of the HAXPES line intensities, an annealing-promoted agglomeration of Ag was suggested to take place in the low-temperature regime. Considering how the HAXPES line intensities evolve in the high-temperature regime in combination with TEM images taken after high-temperature annealing, however, indicate a significant intermixing of Ag and In across the Ag/In$_2$O$_3$:H interface. Detailed line shape analyses reveal that the broadening of the Ag 3d spectra with annealing is attributed to Ag oxidation (i.e., the formation of Ag$_2$O and AgO) becoming significant for annealing temperatures of 160 °C and higher. The significant increase of the In 3d line intensity and its narrowing upon annealing using temperatures >215 °C, is attributed to the promotion of the (inter)diffusion processes, resulting in a reduction of the doping level in In$_2$O$_3$:H.

As a result of these insights, a high-temperature (300 °C instead of the generally used 200 °C) post-annealing treatment of the Ag/In$_2$O$_3$:H contact was performed in order to benefit from the elemental interdiffusion and avoid the formation of an insulating Ag oxide-type interlayer. This indeed led to an improvement of the contact resistance contrary to its often-observed annealing-induced deterioration.

4. Experimental Section

Sample Preparation and Properties: 200-nm thick In$_2$O$_3$:H films were prepared on borosilicate glass substrates by direct current (DC) magnetron sputtering and the introduction of H$_2$O vapor during the process as a hydrogen source. During deposition, the total pressure was about 3 × 10^{-3} mbar, with a water vapor partial pressure of 1 × 10^{-5} mbar. Solid-phase crystallization (SPC) of the deposited In$_2$O$_3$:H films was performed by annealing at 200 °C for 60 min in a vacuum during which the hydrogen content is expected to decrease from ≈4 to 2 at%.[6,16] More details on the preparation of In$_2$O$_3$:H films can be found in a previous publication.[2]

The crystal structure, before and after the SPC annealing procedure, was checked with grazing-incidence X-ray diffraction (GIXRD) using a Bruker ETA diffractometer in the angle-dispersive mode with monochromatic Cu Kα radiation (λ = 1.5405 Å). The comparison with the powder reference patterns of In$_2$O$_3$ (see Figure S1, Supporting Information, for corresponding diffraction data) confirms an annealing-induced SPC of the bare (initially amorphous) In$_2$O$_3$:H film.

Hall-effect measurements of these samples were measured using an Ecopia HMS-3000 Hall system in the van der Pauw configuration; it (Table S1, Supporting Information) reveals a large increase in mobility (μ) from 39.9 to 127 cm^2 V^{-1} s^{-1}, a decrease in carrier concentration (n_e) from 3.86 × 10^{20} to 1.64 × 10^{20} cm^{-3}, and a slight decrease in resistivity (ρ) from 4.05 × 10^{-4} to 2.99 × 10^{-4} Ω cm upon crystallization of the In$_2$O$_3$:H film, in agreement with ref. [2].

Prior to the HAXPES experiments, crystallized In$_2$O$_3$:H was introduced into the combined analysis and deposition UHV system (base pressure <1 × 10^{-9} mbar) of the Energy Materials In situ Laboratory Berlin

ADVANCED
SCIENCE NEWS
www.advancedsciencenews.com

ADVANCED
MATERIALS
INTERFACES
Open Access
www.advmatinterfaces.de

(EMIL).[17] A gentle surface-cleaning process was performed using a mild, low-energy (150 eV) argon ion (Ar$^+$) sputtering of the bare In$_2$O$_3$:H films for 30 min. Before and after sputtering, C 1s, O 1s, and In 3d core levels were measured with laboratory-based X-ray photoelectron spectroscopy (XPS, using a Scienta Omicron Argus CU electron analyzer using Al Kα ($h\nu$ = 1486.58 eV) excitation energy) to monitor the surface cleaning process and ensure that the chemical In$_2$O$_3$:H surface structure was not altered by the sputtering process. Note that no subsequent annealing step was performed as no significant defect formation was expected to be caused by this mild Ar$^+$ sputter treatment. After surface-cleaning, Ag films were prepared on In$_2$O$_3$:H by electron beam evaporation (SPECS EBE-4) of Ag powder without breaking UHV. Based on pre-experiments on In$_2$O$_3$:Sn (not shown), employing a filament current of about 3.32 A for ≈5 min was sufficient to deposit the desired amount of Ag. For the as-prepared Ag/In$_2$O$_3$:H sample, a clear In 3d XPS signal could still be detected, indicating that the thickness of the deposited Ag film was thinner than the XPS probing depth (i.e., about 7 nm at $h\nu$ = 1486.58 eV)[18] and/or does not completely cover the In$_2$O$_3$:H.

Note that in "real-world" applications, thicker Ag layers were deployed. Hence, for the determination of the contact resistance via the transmission line method (TLM, see below) two additional Ag/In$_2$O$_3$:H samples were prepared. For sample 1 (170 ± 20 nm) and sample 2 (330 ± 30 nm), Ag was deposited on the In$_2$O$_3$:H using the same setup as for the thin Ag films. However, in between the deposition of the Ag thin films (for the HAXPES and electron microscopy studies) and the thick Ag layers (for the contact resistance measurements), the e-beam evaporator had to be re-equipped with Ag powder. This is when it was discovered that the Al$_2$O$_3$ crucible used to hold the Ag powder was found to be damaged, and thus was replaced. The deposition time for the thick Ag layers had to be increased to ≈5 h and the sample position was changed relative to the evaporator continuously to ensure complete coverage of the TLM grid mask. After preparation (and initial characterization of the contact resistance), the sample was vacuum annealed at 300 °C for 1 h prior to repeated contact resistance determination. During evaporation and annealing, the pressure in the preparation chamber was around 1 × 10^{-7} mbar. A similarly prepared thick Ag film was used as a reference for the complementing material characterization (see details below).

Sample Characterization: The chemical structure of the Ag/In$_2$O$_3$:H interface and how it changes upon annealing from room temperature to 300 °C was in-situ monitored by HAXPES. The measurements were conducted at the high kinetic energy photoelectron spectrometer (HiKE) endstation[19] located at the BESSY II KMC-1 beamline[20] at Helmholtz-Zentrum Berlin für Materialien und Energie GmbH (HZB), using an excitation energy of 2 keV and a Scienta R4000 electron energy analyzer. The pass energy and energy step width for the core level scans were 200 and 0.1 eV, respectively. All binding energies of the HAXPES spectra were calibrated using Au 4f reference spectra of a clean Au foil, setting the Au 4f$_{7/2}$ to 84 eV. The total energy resolution of the core level spectra was ≈0.25 eV. For sample mounting and transferring between EMIL and HiKE, the samples were sealed, unpacked, and introduced by means of an N$_2$-purged glovebox or glovebag. During the annealing from room temperature to 300 °C (≈8 h duration), 16 HAXPES measurement cycles (of survey and corresponding detail spectra) were performed.

The surface morphology of the bare In$_2$O$_3$:H layer and the Ag/In$_2$O$_3$:H sample after being in situ annealed to 300 °C was studied via SEM using a HITACHI S-4100 system equipped with a cold field emission gun.

A cross-section of the Ag/In$_2$O$_3$:H sample that had been in-situ annealed to 300 °C was additionally studied by TEM and energy dispersive X-ray spectroscopy (EDS). Measurements were performed at the Bundesanstalt für Materialforschung und -prüfung (BAM), Division 6.3 for Structure Analysis using a Thermo Fisher Scientific Talos F200S TEM operating at 200 kV. EDS was performed with two silicon drift detectors (with an energy resolution of ≈120 eV) and 3D chemical characterization with compositional mapping in TEM and scanning TEM (STEM) mode including high-angle annular dark-field imaging (HAADF). Velox software was used for imaging and evaluation. The cross-section of the sample was prepared by face-to-face gluing of two sample

stripes, careful mechanical polishing of the cross-section, and Ar-ion milling.

The sheet resistance of In$_2$O$_3$:H and the contact resistivity of "real-world" Ag/In$_2$O$_3$:H layer stacks in the as-deposited state and after annealing (in vacuum for 1 h at 300 °C, see above) was determined by TLM (see Section S2, Supporting Information, for details). The Ag pads had a length of 0.1 cm, and a width of 0.8 cm and were deposited by electron beam evaporation (see above) through a TLM mask. The distance between the pads varied from 0.12 to 0.32 cm.

Conflict of Interest

The authors declare no conflict of interest.

Data Availability Statement

The data that support the findings of this study are available on request from the corresponding author. The data are not publicly available due to privacy or ethical restrictions.

[1] a) Y. Jiang, T. Feurer, R. Carron, G. T. Sevilla, T. Moser, S. Pisoni, R. Erni, M. D. Rossell, M. Ochoa, R. Hertwig, A. N. Tiwari, F. Fun, *ACS Nano* **2020**, *14*, 7502; b) A. Samanta, J. B. Varley, V. Lordi, *J. Appl. Phys.* **2021**, *129*, 045102.

[2] L. Barraud, Z. Holman, N. Badel, P. Reiss, A. Descoeudres, C. Battaglia, S. De Wolf, C. Ballif, *Sol. Energy Mater. Sol. Cells* **2013**, *115*, 151.

[3] M. Nazarzadehmoafi, S. Machulik, F. Neske, V. Scherer, C. Janowitz, Z. Galazka, M. Mulazzi, R. Manzke, *Appl. Phys. Lett.* **2014**, *105*, 162104.

[4] a) H. von Wenckstern, D. Splith, F. Schmidt, M. Grundmann, O. Bierwagen, J. S. Speck, *APL Mater.* **2014**, *2*, 046104; b) J. Michel, D. Splith, J. Rombach, A. Papadogianni, T. Berthold, S. Krischok, M. Grundmann, O. Bierwagen, H. von Wenckstern, M. Himmerlich, *ACS Appl. Mater. Interfaces* **2019**, *11*, 27073.

[5] R. Xu, J. He, Y. Song, W. Li, A. Zaslavsky, D. C. Paine, *Appl. Phys. Lett.* **2014**, *105*, 093504.

[6] T. Koida, M. Kondo, K. Tsutsumi, A. Sakaguchi, M. Suzuki, H. Fujiwara, *J. Appl. Phys.* **2010**, *107*, 033514.

[7] G. B. Hoflund, Z. F. Hazos, G. N. Salaita, *Phys. Rev. B* **2000**, *62*, 11126.

[8] a) R. G. Egdell, W. Flavell, P. Tavener, *J. Solid State Chem.* **1984**, *51*, 345; b) R. G. Egdell, J. Rebane, T. J. Walker, D. S. L. Law, *Phys. Rev. B* **1999**, *59*, 1792; c) P.-A. Glans, T. Learmonth, K. E. Smith, J. Guo, A. Walsh, G. W. Watson, F. Terzi, R. G. Egdell, *Phys. Rev. B* **2005**, *71*, 235109; d) D. J. Payne, R. G. Egdell, W. Hao, J. S. Foord, A. Walsh, G. W. Watson, *Chem. Phys. Lett.* **2005**, *411*, 181; e) J.-N. Chazalviel, M. Campagna, G. K. Wertheim, H. R. Shanks, *Phys. Rev. B* **1977**, *16*, 697; f) C. Körber, V. Krishnakumar, A. Klein, G. Panaccione, P. Torelli, A. Walsh, J. L. F. Da Silva, S.-H. Wei, R. G. Egdell, D. J. Payne, *Phys. Rev. B* **2010**, *81*, 165207.

[9] a) A. Kotani, Y. Toyozawa, *J. Phys. Soc. Jpn.* **1974**, *37*, 912; b) J.-J. Chang, D. C. Langreth, *Phys. Rev. B* **1973**, *8*, 4638.

[10] A. Walsh, C. R. Catlow, *J. Mater. Chem.* **2010**, *20*, 10438.

[11] a) B. Medasani, Y. H. Park, I. Vasiliev, *Phys. Rev. B* **2007**, *75*, 235436; b) L. Vitos, A. V. Ruban, H. L. Skriver, J. Kollár, *Surf. Sci.* **1998**, *411*, 186.

[12] A. M. Ferraria, A. P. Carapeto, A. M. do Rego, *Vacuum* **2012**, *86*, 1988.

[13] S. Doniach, M. Sunjic, *J. Solid State Phys.* **1970**, *3*, 285.

[14] J. Carper, Bowker Magazine Group Cahners Magazine Divsion 249 W 17TH ST, New York **1999**, p. 124.

[15] P. Reunchan, X. Zhou, S. Limpijumnong, A. Janotti, C. G. Van de Walle, *Curr. Appl. Phys.* **2011**, *11*, S296.

[16] Y. Wu, B. Macco, D. Vanhemel, S. Kölling, M. A. Verheijen, P. M. Koenraad, W. M. M. Kessels, F. Roozeboom, *ACS Appl. Mater. Interfaces* **2017**, *9*, 592.

[17] a) K. Lips, D. E. Starr, M. Bär, T. F. Schulze, F. Fenske, S. Christiansen, R. van de Krol, S. Raoux, G. Reichardt, F. Schäfers, S. Hendel, R. Follath, J. Bahrdt, M. Scheer, G. Wustefeld, P. Kuske, M. Havecker, A. Knop-Gericke, R. Schlogl, B. Rech, in *2014 IEEE 40th Photovoltaic Specialist Conf. (PVSC)*, IEEE, Piscataway, NJ **2014**, pp. 0698–0700; b) R. Félix, N. Llobera-Vila, C. Hartmann, C. Klimm, M. Hartig, R. Wilks, M. Bär, *RSC Adv.* **2018**, *8*, 67.

[18] S. Tanuma, C. J. Powell, D. R. Penn, *Surf. Interface Anal.* **1994**, *21*, 165.

[19] M. Gorgoi, S. Svensson, F. Schäfers, G. Öhrwall, M. Mertin, P. Bressler, O. Karis, H. Siegbahn, A. Sandell, H. Rensmo, W. Doherty, C. Jung, W. Braun, W. Eberhardt, *Nucl. Instrum. Methods Phys. Res. A* **2009**, *601*, 1.

[20] F. Schaefers, M. Mertin, M. Gorgoi, *Rev. Sci. Instrum.* **2007**, *78*, 123102.

2202347 (8 of 8)